Mathematical Geology, Vol. 19, No. 4, 1987

A Mathematical Model of Spheroidal Weathering[1]

R. S. Sarracino,[2] G. Prasad,[3] and M. Hoohlo[2]

A mathematical model is developed to explain the geometrical patterns of spheroidal weathering. The model is then analyzed, and results of computer simulations for the weathering of spherical and ellipsoidal surfaces are presented. Ellipsoids weather initially into ellipsoids of greater or lesser eccentricity, depending on boundary conditions, and finally into spheres. This is in qualitative agreement with the geometry of observed weathering patterns. Some of these features would be difficult to explain by a diffusion model. The weathering of rectangles also is simulated, and they weather into ellipses or circles. These are also in qualitative agreement with observed weathering patterns.

KEY WORDS: Weathering, spheroidal, mathematical modeling, computer simulation.

INTRODUCTION

Spheroidal weathering structures are formed by differential chemical leaching and precipitation in rocks. Weathering starts from a network of fractures and fissures. Water percolates along these and penetrates the polygonal body from all sides, producing concentric ellipsoidal and spherical shells of decayed rock (Figs. 1–3). Weathering cells are typically 0.02–2.00 m in diameter. The weathering front migrates from the outside toward the center. Occasionally a core of unweathered rock is preserved. Microstructure analysis shows that minerals of the unweathered rock are dissolved, elements are mobilized, and some are reprecipitated. Commonly, alternating Fe-rich and Fe-depleted zones occur (Fig. 3). These concentric weathering structures are found in a variety of rock types including granite, basalt, gabbro, sandstone, bauxite, and others (Augustithis and Otteman, 1966; Singer and Navrot, 1970; Augustithis et al., 1980; Augustithis, 1982).

Alternating concentric precipitations were first described by Liesegang (1913). In his experiments, Liesegang produced parallel rings when potassium

[1]Manuscript received 21 May 1986; accepted 8 October 1986.

[2]Department of Physics, National University of Lesotho, PO Roma 180, Lesotho Africa.

[3]Institute of Southern African Studies, National University of Lesotho, PO Roma 180, Lesotho Africa.

0882-8121/87/0500-0269$05.00/1

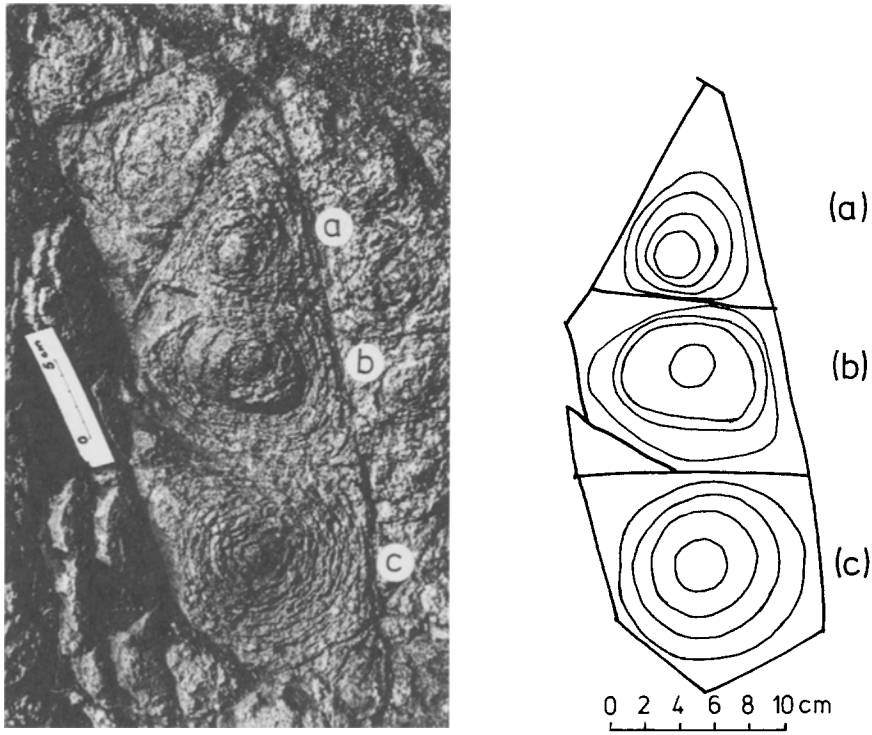

Fig. 1. Typical spheroidal weathering structures. Measurements are made from the line drawing.

dichromate and silver nitrate reacted in gelatin. Silver dichromate precipitated in concentric rings alternating with areas of no precipitation. The rings form by diffusion of silver dichromate through gelatin which forms a barrier to the other salt solution. This phenomenon is called Liesegang diffusion. Liesegang (1913) relates these diffusion rings to Fe-rich banding in weathered rocks and suggests the process of formation might be similar. Carl and Amstutz (1958) experimentally show that Liesegang rings also are formed in three-dimensional bodies with 80–90% quartz grains and 5–10% gelatin; the rings either stop at grain boundaries or deviate around sand grains.

These findings are similar to observations made on natural rocks in which Fe-rich rings terminate at mineral grains or go around them. Carl and Amstutz conclude that the Fe-rich rings in weathered rocks are caused by diffusion and periodic precipitation in a colloidal matrix or intergranular film. Augustithis and Ottemann (1966) show an exchange of elements occurs between the Fe-rich and the Fe-depleted zones in weathered granite. The amount of Ca and Fe increases in brown, Fe-rich zones whereas Al, Si, K, Zr, Y, and Rb are enriched in Fe-depleted zones. They propose two opposing directions of element migration,

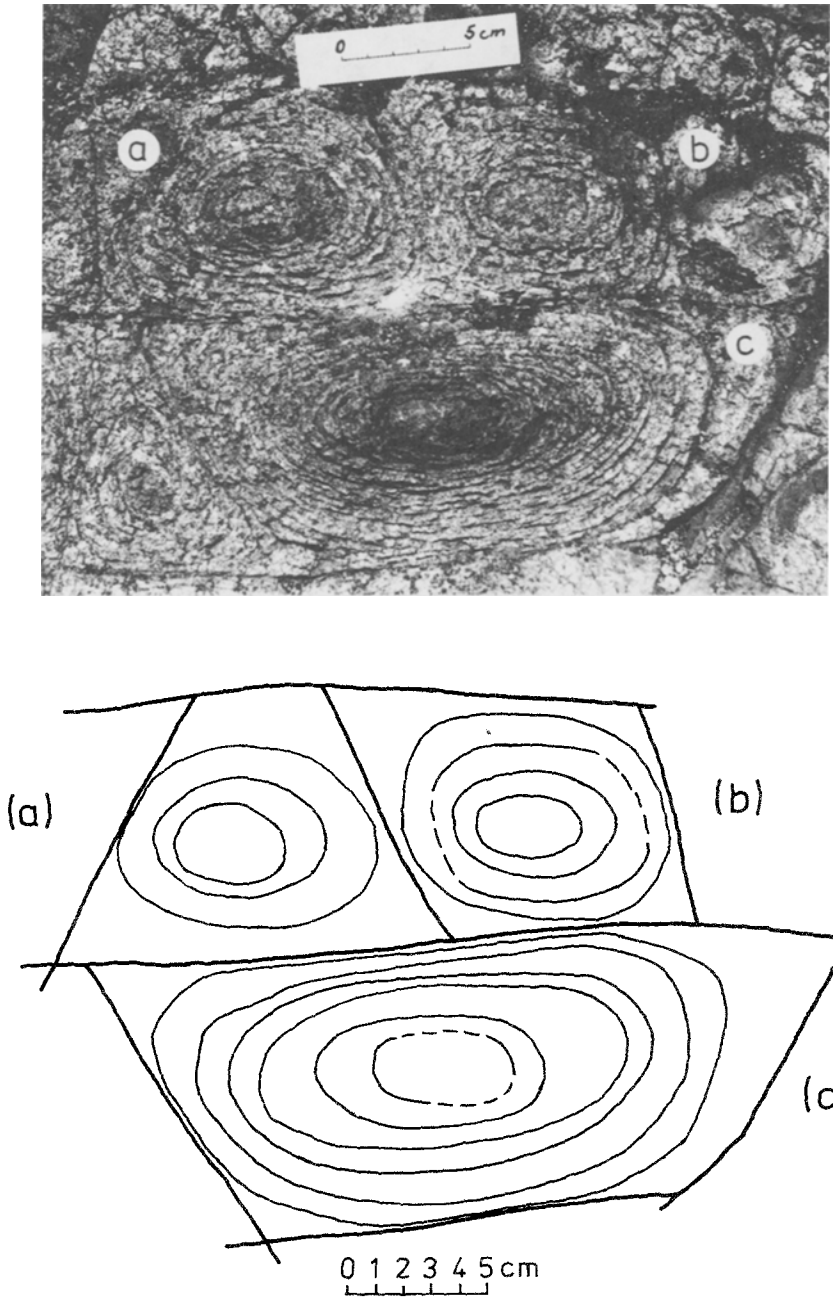

Fig. 2. Ellipsoidal weathering structures become more ellipsoidal and then, toward the center, less so.

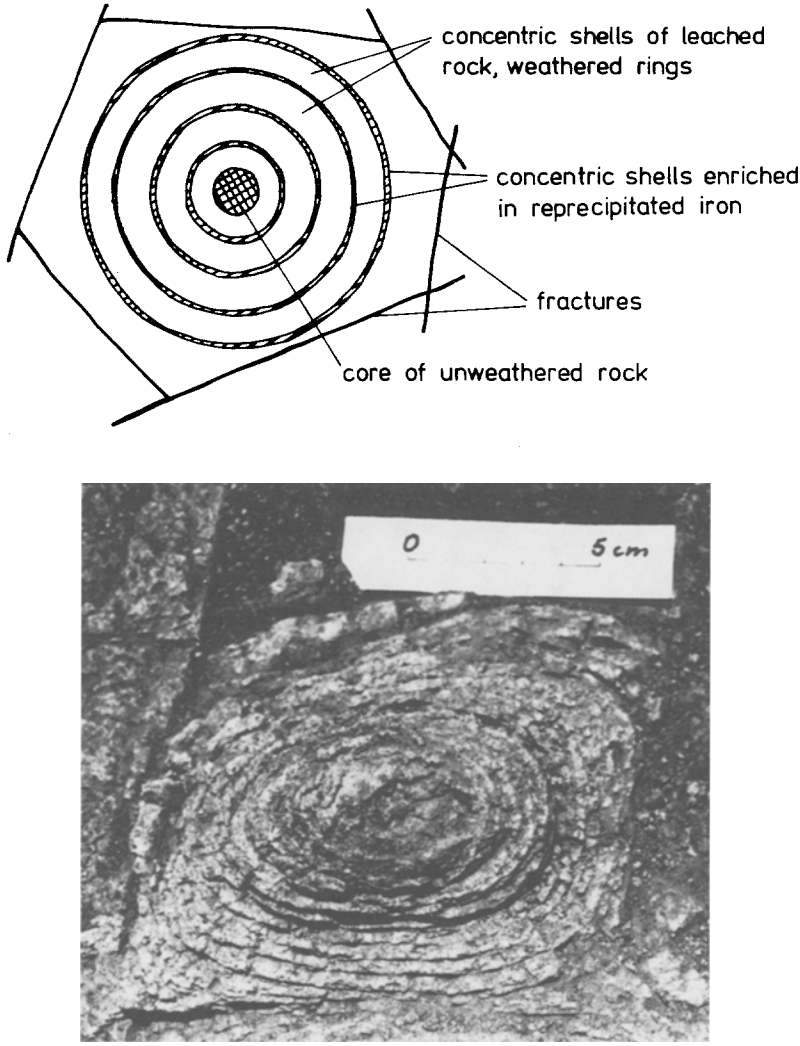

Fig. 3. Schematic section through spheroidal weathering structure. Weathering starts from a network of fractures along which water percolates and penetrates from all sides.

producing a pH environment in which Fe precipitation is effective. The Liesegang phenomenon partially explains this process.

Singer and Navrot (1970) study the mineralogical and chemical alterations accompanying formation of diffusion rings in a basalt boulder. Depletion of Fe from the white core is explained by little stability of mafic minerals and a reducing environment. Accumulation of Fe in the brown rings is attributed to a rise in Eh due to fissuring of the rock. In more recent work, diffusion rings in

bauxites and other rocks are analyzed, and elemental leaching and mobilization are proposed to be the mechanisms for formation of diffusion rings (Augustithis et al., 1980; Augustithis, 1982).

In the above experiments, diffusion is in one direction, either from inside to outside as in the two-dimensional experiment of Liesegang (1913) or from outside to inside, as in the three-dimensional case of Carl and Amstutz (1958). The diffusion medium also is assumed to be homogeneous. Spheroidal weathering in nature is in two directions, and the medium is generally not homogeneous. Solution penetrates a rock from the outside to the weathered/fresh rock interface whereas leached elements are carried away from the interface to the outside.

During this weathering process, three types of spheroids are formed: (1) the unweathered cores, (2) the decomposed and leached Fe-depleted shells, and (3) reprecipitated Fe-rich zones (Fig. 3). Among these types of spheroid formation only the third, or reprecipitated Fe-rich zones, is formed by a process similar to the Liesegang phenomenon (Matalon and Packter, 1955; Packter, 1956a, 1956b). The interface between unweathered core and weathered rock cannot be formed by diffusion because fresh rock is impermeable to water. On the scale with which we are dealing, the interface presents a sharp discontinuity in mineral and water concentration and would, therefore, propagate in a fashion analogous to that of a shock front.

Because the geometry of the first two spheroid types is not in accord with the Liesegang-type diffusion rings, but is consistent with the geometry one would expect from the propagation of a discontinuity interface, we suggest that the geometry of weathering patterns is determined by the geometry of the shrinking interface, and not by diffusion.

These considerations have led to a shock-front model involving propagation of a discontinuity (in this case the interface), in an attempt to explain the geometry of weathering rings. We introduce and analyze a general mathematical model for the shape of weathering fronts, which leads to both the ellipsoidal and spheroidal weathering observed in nature, and we justify the overall predictions of the model through measurements of a number of selected, representative weathering structures.

PRELIMINARY CONSIDERATIONS

On cut and exposed rock faces one can see the network of original fissures and the weathering pattern. The weathering surface rapidly evolves from a polygon into concentric ellipses, of increasing (Figs. 1b; 2b,c) and decreasing (Figs. 1a,c; 2a) eccentricity. Whether or not the eccentricity initially increases, it eventually decreases (e.g. Figs. 1b and 2c), and the ellipses weather into concentric circles. Because the observed face presents sections from randomly ori-

ented cuts through the weathered structure, we conclude an initial irregular polygonal body will weather into an ellipsoid and eventually into a sphere. Any viable model would have to explain this phenomenon of both spherical and ellipsoidal weathering.

The time scale for weathering is large. We assume that no considerable change occurs in water concentration during the weathering process and that fissures are adequately narrow. Structures are assumed far enough below the surface, that at the scale of the individual structure, capillary action would overcome the effect of the gravitational field gradient, so that weathering rates would be expected to be independent of cell orientation. On a scale less than a tenth of a millimeter, the fresh/weathered rock interface is complicated. However, on the scale we are dealing with, inhomogeneities of rock texture and crystal orientation and size are averaged out, so that fresh rock presents a homogeneous face to the water. Hence, the direction of weathering would parallel the geometric gradient of the interface surface at each point, and the propagation rate for a given rock in a given environment would depend solely on the local geometry of the surface. These considerations have lead to the model presented here.

THE MATHEMATICAL MODEL

Let the fresh surface be represented by a function of three spatial coordinates and time

$$f(x(t), y(t), z(t)) = c(t) \tag{1}$$

Function f represents a three-dimensional surface embedded in a four-dimensional x, y, z, t space, points of which can be characterized by three parameters s, u, and t. A surface point $P(t_0, s_0, u_0)$, with spatial coordinates $x(t_0, s_0, u_0)$, $y(t_0, s_0, u_0)$, and $z(t_0, s_0, u_0)$, on the two-dimensional surface

$$f[x(t_0), y(t_0), z(t_0)] = c(t_0) \tag{2}$$

is considered to weather into point $P(t_1, s_0, u_0)$, with coordinates $x(t_1, s_0, u_0)$, $y(t_1, s_0, u_0)$, and $z(t_1, s_0, u_0)$, which lies on the neighboring surface

$$f[x(t_1), y(t_1), z(t_1)] = c(t_1) \tag{3}$$

If $t_1 - t_0$ is infinitesimal, Δt, the vector separating $P(t_0, s_0, u_0)$ and $P(t_1, s_0, u_0)$, is

$$\frac{-F(r)\,\nabla f}{|\nabla f|}(t_1 - t_0) \tag{4}$$

where ∇f is a gradient of $c(t_0)$ at $P(t_0, s_0, u_0)$, and $F(r)$ is some function of r, the radius of curvature of $c(t_0)$ at $P(t_0, s_0, u_0)$.

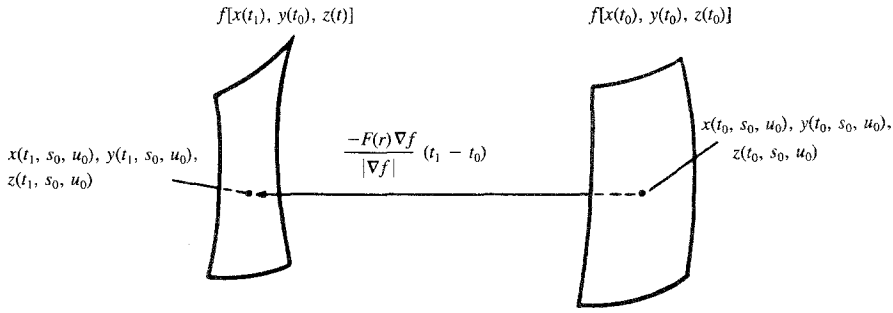

Scheme I

The negative sign arises because on a convex surface the gradient vector is opposite to the weathering direction. A contracting surface implies $c(t_1) < c(t_0)$; therefore, we find that

$$\begin{aligned} & f[x(t_1, s_0, u_0), y(t_1, s_0, u_0), z(t_1, s_0, u_0)] \\ & \quad - f[x(t_0, s_0, u_0), y(t_0, s_0, u_0), z(t_0, s_0, u_0)] \\ & = \left(\frac{\delta f}{\delta x}\frac{dx}{d(t)} + \frac{\delta f}{\delta y}\frac{dy}{dt} + \frac{\delta f}{\delta z}\frac{dz}{dt}\right)(t_1 - t_0) = \frac{dc}{dt}(t_1 - t_0) < 0 \\ & \equiv (f_x\dot{x} + f_y\dot{y} + f_z\dot{z})(t_1 - t_0). \end{aligned} \tag{5}$$

We also note

$$x(t_1, s_0, u_0) - x(t_0, s_0, u_0) = \frac{\delta x}{\delta t}(t_1 - t_0) = \frac{-F(r)f_x}{|\nabla f|}(t_1 - t_0). \tag{6}$$

Substituting (6) into (5), we obtain

$$\frac{-F(r)(f_x^2 + f_y^2 + f_z^2)}{|\nabla f|} = -F(r)(f_x^2 + f_y^2 + f_z^2)^{1/2} = \dot{c} < 0. \tag{7}$$

Without loss of generality, we can set $\dot{c} = -k$, where k is a positive constant. Equation (7) then becomes a nonlinear first-order partial differential equation in three independent variables

$$G(x, y, z, f, p, q, w) = -F[r(x, y, z)](p^2 + q^2 + w^2)^{1/2} + k = 0 \tag{8}$$

with a solution characterized by three parameters, t, s, and u. There will be $(2n + 1) = 7$ equations for the characteristics of the partial differential equation

$$\frac{dx}{dt} = \frac{\delta G}{\delta p} = \frac{-F^2 p}{k} \qquad \frac{dy}{dt} = \frac{\delta G}{\delta q} = \frac{-F^2 q}{k} \qquad \frac{dz}{dt} = \frac{\delta G}{\delta w} = \frac{-F^2 w}{k}$$

$$\frac{df}{dt} = p\frac{\delta G}{\delta p} + q\frac{\delta G}{\delta q} + w\frac{\delta G}{\delta w} = -k$$

$$\frac{dp}{dt} = -\frac{\delta G}{\delta x} - p\frac{\delta G}{\delta f} = \frac{-\delta G}{\delta x} = \frac{kF_x}{F} \qquad \frac{dq}{dt} = \frac{kF_y}{F} \qquad \frac{dw}{dt} = \frac{kF_z}{F} \tag{9}$$

For a given problem, we prescribe the initial conditions

$$f = f(t_0, s, u) \qquad x = x(t_0, s, u)$$

$$y = y(t_0, s, u) \qquad z = z(t_0, s, u) \tag{10}$$

and can determine the initial conditions for the dependent variables $p = p(t_0, s, u)$, $q = q(t_0, s, u)$, and $w = w(t_0, s, u)$, from the three equations

$$\frac{\delta f}{\delta s} = p\frac{\delta x}{\delta s} + q\frac{\delta y}{\delta s} + w\frac{\delta z}{\delta s}$$

$$\frac{\delta f}{\delta u} = p\frac{\delta x}{\delta u} + q\frac{\delta y}{\delta u} + w\frac{\delta z}{\delta u}$$

$$G\big|_{t_0, s, u} = 0 \tag{11}$$

As a criterion for uniqueness of the solution, the initial conditions must be such that the determinant

$$J = \begin{vmatrix} \frac{\delta G}{\delta p} & \frac{\delta G}{\delta q} & \frac{\delta G}{\delta w} \\ \frac{\delta x}{\delta s} & \frac{\delta y}{\delta s} & \frac{\delta z}{\delta s} \\ \frac{\delta x}{\delta u} & \frac{\delta y}{\delta u} & \frac{\delta z}{\delta u} \end{vmatrix} \neq 0 \tag{12}$$

The final step is to evaluate the function $F(r)$. Assuming the rock to be homogeneous, composition of fresh rock on one side of the interface and weathered rock on the other side are independent of time because, on the weathering time-scale, the weathering interface propagates in a fashion analogous to a shock front. Therefore, weathering rate will depend solely on the geometry of the interface.

What is the probability that a given molecule will be pulled out of the fresh rock by solution at the interface? The molecule is held in place by neighboring molecules in the rock while being attracted into solution by the surrounding water molecules. The net weathering rate at a point on the interface should then be directly proportional to the ratio of the solid angles of the outer and inner faces.

$$F(r) = \frac{\text{solid angle of } H_2O \text{ surrounding rock section}}{\text{solid angle of rock at section}} = \frac{\Omega_{H_2O}}{4\pi - \Omega_{H_2O}} \quad (13)$$

A number of functions can be used to relate the radius of curvature r and Ω, each characterized by a different distance scale. For instance, one possible relationship is given by

$$\Omega_{H_2O} = 2\pi(1 + e^{-r}) \quad (14)$$

This has the necessary limits: 2π for $r = \infty$ (a plane) and 4π for $r = 0$ (a point). From Eq. (14)

$$F(r) = \frac{1 + e^{-r}}{1 - e^{-r}} \quad (15)$$

We choose a more convenient relationship

$$\Omega_{H_2O} = 2\pi\left\{2 - \left[1 + (1/r)\right]^{-1}\right\} \quad (16)$$

which has the same limits as Eq. (14). From Eq. (16)

$$F(r) = 1 + (2/r) \quad (17)$$

Substituting Eq. (17) into Eq. (9) yields the equations for a general three-dimensional weathering surface

$$\frac{dx^i}{dt} = -\frac{1}{k}\left(1 + \frac{2}{r}\right)^2 p^i$$

$$\frac{df}{dt} = -k$$

$$\frac{dp^i}{dt} = \frac{-2kr^i}{2r + r^2} \quad (18)$$

where $r^i = dr/dx^i$ and $x^1, x^2, x^3, p^1, p^2, p^3 = x, y, z, p, q, w$.

Radius of curvature is defined unambiguously on any point of a line, but not at any point of a surface. The definition we use is

$$r = \frac{1}{k_0} \quad (19)$$

where k_0, mean curvature, is the average of curvatures of the most strongly and most weakly curved lines on the surface intersecting the particular point. For a surface described by a function f, mean curvature is given by

$$k_0 = \frac{1}{2|\nabla f|^3}\left[f_{xx}(f_y^2 + f_z^2) + f_{yy}(f_x^2 + f_z^2) + f_{zz}(f_x^2 + f_y^2) - 2f_{yz}f_yf_z - 2f_{xz}f_xf_z - 2f_{xy}f_xf_y\right] \quad \text{where} \quad (20)$$

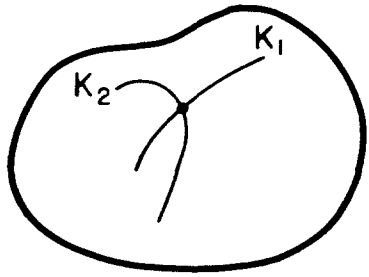

Scheme II

$$f_x = \frac{\delta f}{\delta x} \qquad f_{xy} = \frac{\delta^2 f}{\delta x\, \delta y} \qquad \text{etc.} \tag{21}$$

WEATHERING OF A PLANE

Exact solutions to Eq. (18) will now be found for a plane and a sphere. Choosing a convenient orientation of coordinate axes, a plane may be parameterized by

$$x(t_0, s, u) = s \qquad y(t_0, s, u) = u \qquad z(t_0, s, u) = t_0 \qquad f = 0 \tag{22}$$

The radius of curvature is infinite, so that $F = 1$. From Eq. (11), we find

$$p(t_0, s, u) = 0 \qquad q(t_0, s, u) = 0 \qquad w(t_0, s, u) = k \tag{23}$$

so that Eq. (18) reduces to

$$\frac{dx}{dt} = 0 \qquad \frac{dy}{dt} = 0 \qquad \frac{dz}{dt} = \frac{-w}{k}$$

$$\frac{dp}{dt} = \frac{k}{F}\frac{\delta F}{\delta x} = 0 \qquad \frac{dq}{dt} = 0 \qquad \frac{dw}{dt} = 0 \tag{24}$$

with the solution

$$x = s \qquad y = u \qquad z = t_0 - t \tag{25}$$

which is the equation of a plane discontinuity moving perpendicularly to the z axis.

WEATHERING OF A SPHERE

The initial coordinates are given by

$$x = a_0 \cos s \sin u \qquad y = a_0 \sin s \sin u \qquad z = a_0 \cos u \qquad f = \text{const.} \tag{26}$$

with

$$r(t_0, s, u) = a_0 \tag{27}$$

From Eq. (11), we find

$$0 = -a_0 p \sin s \sin u + a_0 q \cos s \sin u$$

$$0 = a_0 p \cos s \cos u + a_0 q \sin s \cos u - a_0 w \sin u$$

$$0 = \left(1 + \frac{2}{a_0}\right)(p^2 + q^2 + w^2)^{1/2} - k \tag{28}$$

which reduce to

$$p(t_0, s, u) = \frac{k \cos s \sin u}{(1 + 2/a_0)}$$

$$q(t_0, s, u) = \frac{k \sin s \sin u}{(1 + 2/a_0)} \qquad w(t_0, s, u) = \frac{k \cos u}{(1 + 2/a_0)} \tag{29}$$

We expect spherical weathering, so

$$x(t, s, u) = a(t) \cos s \sin u \qquad y(t) = a(t) \sin s \sin u$$

$$z(t) = a(t) \cos u$$

$$p(t, s, u) = \frac{k \cos s \sin u}{[1 + 2/a(t)]} \qquad q(t, s, u) = \frac{k \sin s \sin u}{[1 + 2/a(t)]}$$

$$w(t, s, u) = \frac{k \cos u}{[1 + 2/a(t)]} \tag{30}$$

Substituting Eq. (30) into Eq. (18), we obtain

$$\frac{da}{dt} = -[1 + (2/a)] \tag{31}$$

The solution to this first-order differential equation is

$$\left(\frac{2 + a}{2 + a_0}\right)^2 e^{a - a_0} = e^{-(t - t_0)} \tag{32}$$

THE EQUATIONS OF AN ELLIPSOID

We now examine equations for an ellipsoidal surface. Ellipses are the most common weathering curves, suggesting that irregular solids rapidly weather into ellipsoids. We begin with an ellipsoidal surface centered at the origin, with axes parallel to the coordinate axes and with axis radii $a > b > c$.

At $t = t_0$, let the ellipsoid surface be

$$\frac{x^2}{a^2} + \frac{y^2}{b^2} + \frac{z^2}{c^2} = 1 \tag{33}$$

The initial coordinate values are

$$x(t_0, s, u) = a_0 \cos s \sin u$$
$$y(t_0, s, u) = b_0 \sin s \sin u \qquad z(t_0, s, u) = c_0 \cos u \tag{34}$$

Substituting into Eq. (11), and noting $f = \text{const.}$, we obtain

$$0 = -pa_0 \sin s \sin u + qb_0 \cos s \sin u$$
$$0 = pa_0 \cos s \cos u + qb_0 \sin s \cos u - wc_0 \sin u$$
$$0 = \left[1 + (2/a_0)\right](p^2 + q^2 + w^2)^{1/2} - k \tag{34}$$

which gives

$$p(t_0, s, u) = kb_0c_0 \cos s \sin u \Big/ \left\{\left[1 + (2/r_0)\right] \varphi(s, u)\right\}$$
$$q(t_0, s, u) = ka_0c_0 \sin s \sin u \Big/ \left\{\left[1 + (2/r_0)\right] \varphi(s, u)\right\}$$
$$w(t_0, s, u) = ka_0b_0 \cos u \Big/ \left\{\left[1 + (2/r_0)\right] \varphi(s, u)\right\} \qquad \text{where} \tag{36}$$
$$\varphi(s, u) = (b_0^2c_0^2 \cos^2 s \sin^2 u + a_0^2c_0^2 \sin^2 s \sin^2 u + a_0^2b_0^2 \cos^2 u)^{1/2}$$

and (37)

$$r_0 = 2a_0^2b_0^2c_0^2\left(\frac{x_0^2}{a_0^4} + \frac{y_0^2}{b_0^4} + \frac{z_0^2}{c_0^4}\right)^{3/2} \Bigg/ \left[\frac{x_0^2}{a_0^2}(b_0^2 + c_0^2) + \frac{y_0^2}{b_0^2}(a_0^2 + c_0^2) + \frac{z_0^2}{c_0^2}(a_0^2 + b_0^2)\right] \tag{38}$$

Numerical solution of differential equations in Eq. (18) with initial conditions of Eqs. (33–38) is difficult because, as the ellipsoid shrinks, the equations become stiff, and special methods must be used to solve them. However, the equations may be simplified.

Intuitively, we expect the ellipsoid to weather into an ellipsoid (of different eccentricity), represented by

$$x(t, 0, \pi/2) = a(t) \qquad y(t, \pi/2, \pi/2) = b(t) \qquad z(t, s, 0) = c(t) \tag{39}$$

One might think the general solution is represented by

$$x = a(t) \cos s \sin u \quad y = b(t) \sin s \sin u \qquad z = c(t) \cos u \tag{40}$$

However, Eq. (40) would not be a solution because, in general, a weathering path would not be a locus of constant s, u points, as s and u are defined in Eq. (40). Along an axis, the weathering path will be a straight line and is the locus of constant s, u points, as given by Eq. (39). Along the x axis ($s = 0$, $u = \pi/2$), the initial conditions Eqs. (34–38) become

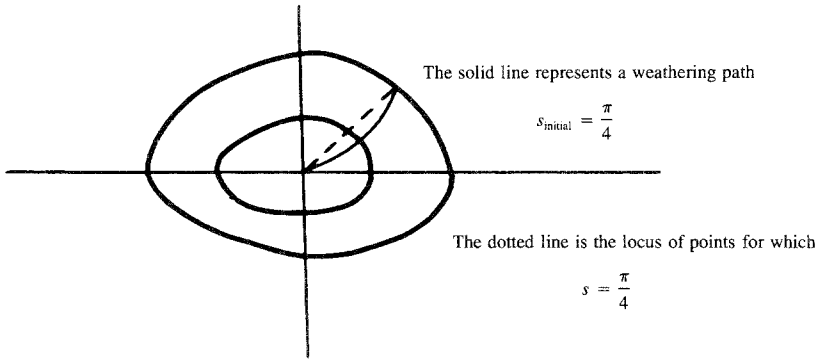

Scheme III

$$x(t_0, 0, \pi/2) = a_0 \qquad y(t_0, 0, \pi/2) = 0 \qquad z(t_0, 0, \pi/2) = 0$$

$$r_0 = \frac{2b_0^2c_0^2}{a_0(b_0^2 + c_0^2)}$$

$$p(t_0, 0, \pi/2) = \frac{k}{1 + (2/r_0)} \qquad q(t_0, 0, \pi/2) = 0 \qquad w(t_0, 0, \pi/2) = 0 \tag{41}$$

Noting that

$$r_s = \frac{2xa^2b^2c^2\left[(x^2/a^4) + (y^2/b^4) + (z^2/c^4)\right]^{1/2}}{\left[(x^2/a^2)(b^2 + c^2) + (y^2/b^2)(a^2 + c^2) + (z^2/c^2)(a^2 + b^2)\right]^2} \cdot \left\{\frac{x^2}{a^6}(b^2 + c^2) + \frac{y^2}{a^2b^2}\left(1 + \frac{3c^2}{a^2} - \frac{2c^2}{b^2}\right) + \frac{z^2}{a^2c^2}\left(1 + \frac{3b^2}{a^2} - \frac{2b^2}{c^2}\right)\right\} \tag{42}$$

we have

$$r_x(t_0, 0, \pi/2) = 2b_0^2c_0^2/a_0^2(b_0^2 + c_0^2) \tag{43}$$

From Eq. (26) and Eq. (18)

$$\left.\frac{da(t)}{dt}\right|_{t_0} = -\left[1 + \frac{a_0(b_0^2 + c_0^2)}{b_0^2c_0^2}\right] \tag{44}$$

Equation (44) is preserved throughout the weathering process. By using similar derivations for the weathering paths, $s = \pi/2$, $u = \pi/2$, and $u = 0$, we find

$$\frac{da}{dt} = -\left[1 + \frac{a(b^2 + c^2)}{b^2c^2}\right] \quad \frac{db}{dt} = -\left[1 + \frac{b(a^2 + c^2)}{a^2c^2}\right]$$
$$\frac{dc}{dt} = -\left[1 + \frac{c(a^2 + b^2)}{a^2b^2}\right] \tag{45}$$

Considering

$$a \geq b \geq c$$
$$a = a[b(c)]$$
$$b = b(c) \tag{46}$$

Eq. (45) becomes

$$\frac{da}{db} = \frac{a^2}{b^2}\left(\frac{ab^2 + ac^2 + b^2c^2}{a^2b + a^2c^2 + bc^2}\right)$$
$$\frac{db}{dc} = \frac{b^2}{c^2}\left(\frac{a^2b + a^2c^2 + bc^2}{a^2b^2 + a^2c + b^2c}\right)$$
$$\frac{da}{dc} = \frac{a^2}{c^2}\left(\frac{ab^2 + ac^2 + b^2c^2}{a^2b^2 + a^2c + b^2c}\right) \tag{47}$$

Of critical importance are the conditions

$$\frac{da}{db} = \frac{a}{b} \quad \frac{db}{dc} = \frac{b}{c} \tag{48}$$

because

$$\frac{da}{db} > \frac{a}{b} \quad \text{and} \quad \frac{db}{dc} > \frac{b}{c} \tag{49}$$

will lead to spheroidal weathering (that is, an ellipsoid will weather into a sphere), whereas

$$\frac{da}{db} < \frac{a}{b} \quad \text{and} \quad \frac{db}{dc} < \frac{b}{c} \tag{50}$$

will lead to ellipsoidal weathering (an ellipsoid will become more eccentric), and mixed conditions will give the appearance of both, depending upon which plane of the cell has been cut. We note for a sphere $a = b = c$

$$\frac{da}{db} = \frac{db}{dc} = 1 \tag{51}$$

so a sphere will remain a sphere, as we expect.

Will the sphere be stable? Let $b = c(1 + \epsilon)$ and $a = b(1 + \delta) = c(1 + \epsilon + \delta)$, to the first order, where

$$(1, 1) \gg (\epsilon, \delta) > (0, 0) \tag{52}$$

Equation (47) becomes

$$\left.\begin{aligned} \frac{db}{dc} = \frac{c + 2(1 - \delta)}{c + 2(1 - 2\epsilon - \delta)} \end{aligned}\right\} \begin{array}{ll} > b/c & c < 2 \\ = b/c & \text{if } c = 2 \\ < b/c & c > 2 \end{array}$$

$$\left.\begin{aligned} \frac{da}{db} = \frac{c + 2(1 + \delta)}{c + 2(1 - \delta)} \end{aligned}\right\} \begin{array}{ll} > a/b & c < 2 \\ = a/b & \text{if } c = 2 \\ < a/b & c > 2 \end{array} \tag{53}$$

Hence, spherical weathering is stable for a sphere smaller than a critical radius.

Will weathering be spheroidal in its final stages? An analysis similar to that above suggests that it will be. Weathering of an ellipsoid is summarized in Table 1.

Equation (45) is nonstiff. They were solved by a Runge–Kutta fourth-order method (Burden et al., 1981). Computer simulations for different planar cuts (Fig. 4a–e) are presented with different initial values of ellipsoid axis length.

WEATHERING FROM AN INITIAL POLYGON

Equations (8)–(17) readily lend themselves to curve evolution from an initial polygon. Because a unique circle can be drawn through any three points, a

Table 1. Type of Weathering as a Function of Axis Length

c (z axis)	b (y axis)	a (x axis)	Type of weathering
>2	$>c$	$>b$	Elliptical in planes through all pairs of axes
>2	$=c$	$=b$	Unstable (spheroidal)
<2	$=c$	$=b$	Stable (spheroidal)
Between 1 and 2	$>c$	$>b$	May be spherical or elliptical through any pair of axes (includes the possibility of mixed weathering)
	$>c/(c-1)$	$[>c/(c-1)]$	Elliptical through the y–z [x–z] axis
	$<c/(c-1)$	$[<c/(c-1)]$	Spherical through the y–z [x–z] axis
<1			Spherical through the x–z and y–z axis
<2		$>b/(b-1)$	Elliptical through the x–y axis
		$<b/(b-1)$	Spherical through the x–y axis

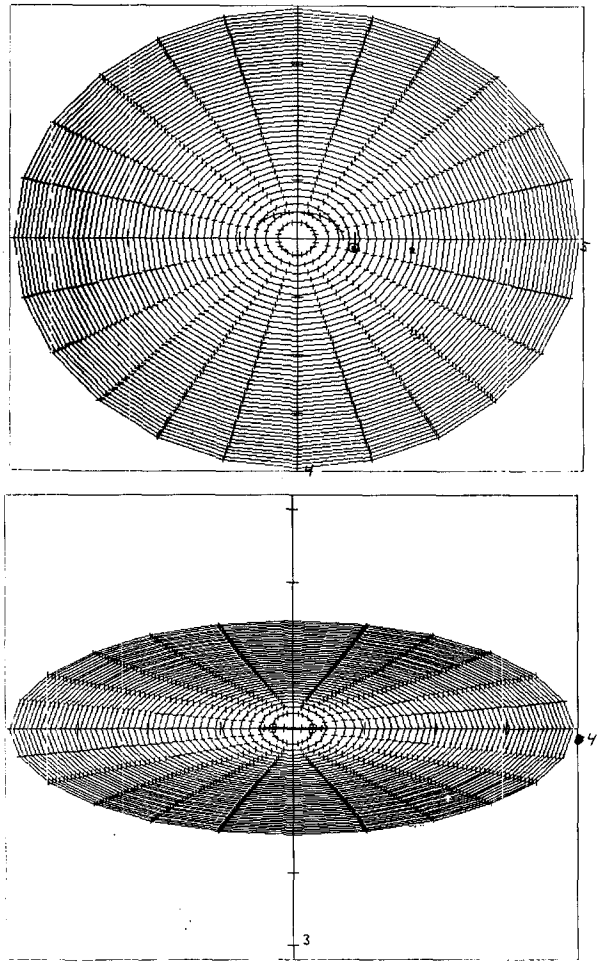

Fig. 4. (a) Computer simulation of weathering in the x–y plane for an ellipsoid with initial axis half-lengths $x = 5$, $y = 4$, $z = 1.5$. Successive ellipses become first more eccentric, then less eccentric. (b) Computer simulation of weathering in the y–z plane for the ellipsoid of (a). (c) Computer simulation of weathering in the x–z plane for the ellipsoid of (a). As is the case in (a) and (b), successive ellipses are first more eccentric, but then weather into less eccentric ellipses. (d) Computer simulation of weathering in the y–z plane for an ellipsoid with initial half-lengths $x = 3$, $y = 2$, $z = 1.5$. Successive ellipses become less eccentric. (e) Computer simulation of weathering in the y–z plane for an ellipsoid with initial half-lengths $x = 1$, $y = 0.8$, $z = 0.6$. Successive ellipses become less eccentric.

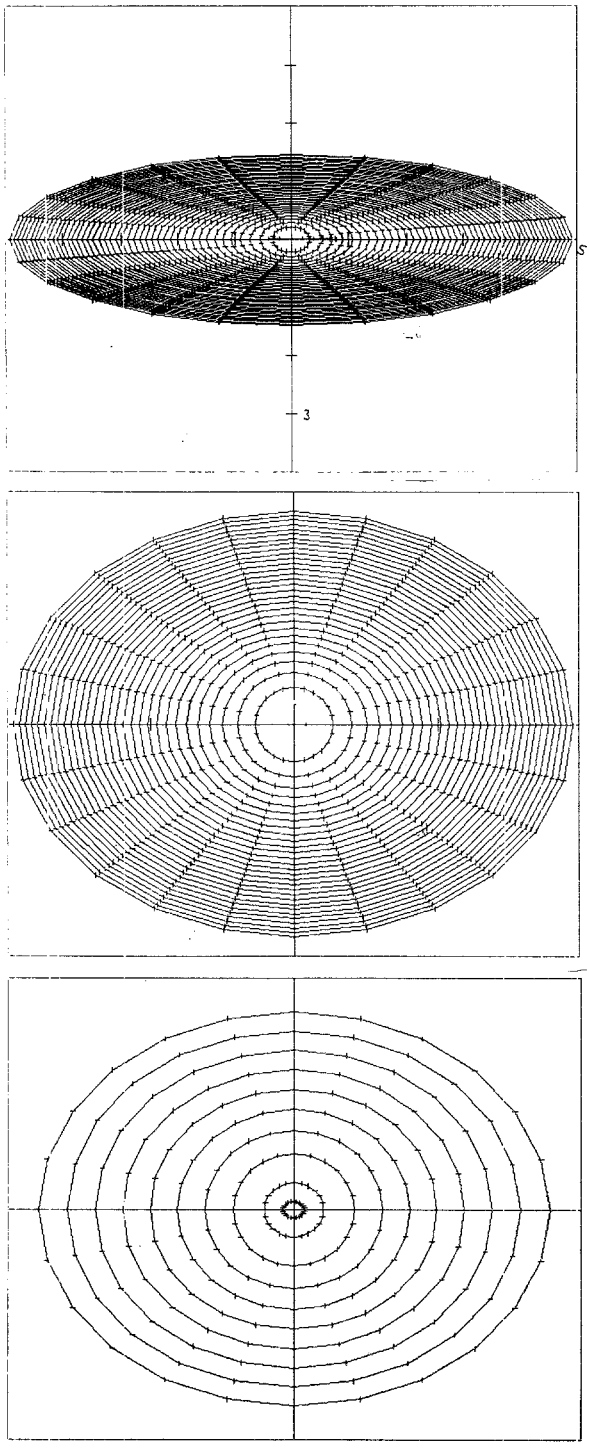
5
3

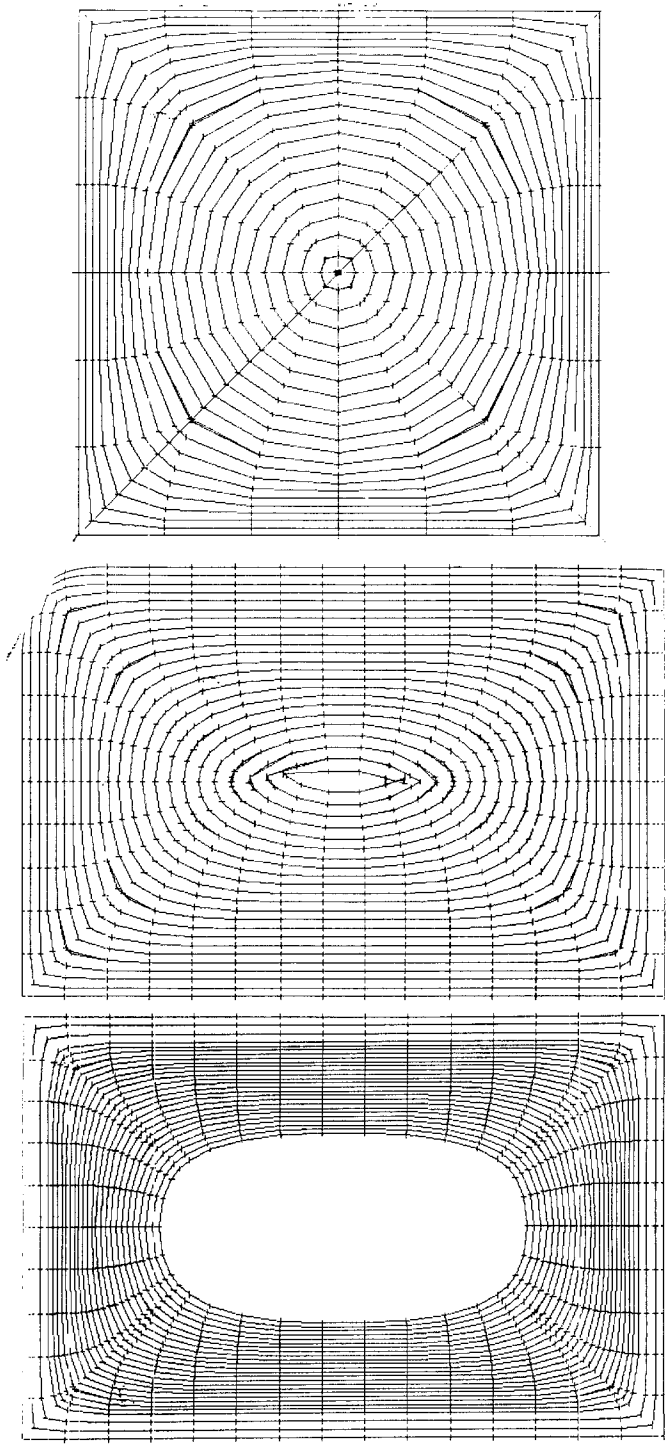

Fig. 5. (a) Computer simulation of weathering from an initial square into a circle. (b) Computer simulation of weathering from an initial rectangle. (c) Computer simulation of weathering from an initial rectangle. The initial rectangle is twice the size as that of (b).

"radius of curvature" can be obtained at any point in a curve. Simulation from an initial rectangle (Fig. 5) clearly shows that the rectangle rapidly evolves into an ellipse-like curve.

The three-dimensional case is not as straightforward because one must average over curves through a point on the surface to obtain a net "radius of curvature." Clearly, however, the overall effect is the same as that for the two-dimensional case.

OBSERVATIONS

A statistical analysis of measurements for weathered structures chosen at random would be a prodigious task. Accordingly, measurements of 14 selected structures, chosen both for the clarity of their rings and for ease of measurement illustrate features of the model (Table 2). The width of the weathered rings seems to depend on grain size and does not appear to represent equal intervals of time. Hence, we have looked at the evolution of the ellipse's shape and not at the distance between successive surfaces. Because chips break off the original structures and parallel cracks develop, the measurements begin with the first recognizable ellipse and not with the original fissure. Uncertainty associated with each measurement is 0.5 mm which leads, in some cases, to relatively large uncertainties in axis ratios.

Of 14 entries (Table 2), entries 1–7 show spherical weathering, that is, the eccentricity of the weathering surface decreases monotonically. Entries 8–14 illustrate elliptical weathering. The eccentricities of the weathering ellipses increase initially and then, for entries 11–14, decrease. Considering uncertainties, entries 2–7 may also belong to this category.

CONCLUSION

Results obtained by the model are in qualitative agreement with observed weathering patterns. A comparison of Fig. 5 with Figs. 1 and 2 shows good agreement with model predictions regarding rapid evolution of the original polygonal body into an ellipse. Perhaps more striking is the agreement of entries 11–14 in Table 2 with predictions of the model. These measurements would be difficult to explain by diffusion.

The model proposed here has the advantage of simplicity. Although clearly an idealization and based on a minimum number of general assumptions, the model reproduces the geometry of weathering patterns observed in nature.

Through a statistical analysis of measurements taken from randomly cut, two-dimensional sections of weathering patterns, the applicability of the model could be conclusively tested. Through such a study, parameters of the model could be fixed and hence relative weathering rates for different rocks, and rocks within different environments, could be obtained.

Table 2. Dimensions and Eccentricities of Successive Ellipses and Circles

Number	Ellipse and circle dimensions in *mm* (±0.5) (major axis/minor axis)			
1 (Fig. 1c)	38/36 1.06 ± 0.02	30/28 1.07 ± 0.03	22/21 1.05 ± 0.05	10/10 1.00 (± 0.10)
2	59/53 1.11 ± 0.02	49/46 1.07 ± 0.02	24/22 1.09 ± 0.05	
3 (Fig. 1a)	26/25 1.04 ± 0.04	21/19 1.11 ± 0.05	15/14 1.07 ± 0.07	10/9 1.11 ± 0.11
4	28/21 1.33 ± 0.06	20/16 1.25 ± 0.07	15/12 1.25 ± 0.09	
5	33/21 1.57 ± 0.06	28/19 1.47 ± 0.06	18/13 1.38 ± 0.09	
6 (Fig. 4a)	45/31 1.45 ± 0.04	30/21 1.43 ± 0.06	20/14 1.43 ± 0.09	
7	48/36 1.33 ± 0.03	41/30 1.37 ± 0.04	28/23 1.22 ± 0.05	14/12 1.17 ± 0.11
8 (Fig. 4b)	46/35 1.31 ± 0.04	37/27 1.37 ± 0.04	29/18 1.61 ± 0.07	19/10 1.90 ± 0.14
9	45/32 1.41 ± 0.03	37/26 1.42 ± 0.04	20/11 1.82 ± 0.12	
10	69/56 1.23 ± 0.02	46/29 1.59 ± 0.04	25/15 1.67 ± 0.09	
11 (Fig. 4c)	99/47 2.11 ± 0.03	87/41 2.12 ± 0.04	74/33 2.24 ± 0.05	65/27 2.41 ± 0.06
		40/19 2.11 ± 0.08	25/13 1.92 ± 0.11	
12	102-96/58 1.71 ± 0.06	85/48 1.77 ± 0.03	68/33 2.06 ± 0.05	33/18 1.83 ± 0.07
13	80/62 1.29 ± 0.02	68/52 1.31 ± 0.02	44/32 1.38 ± 0.04	32/25 1.28 ± 0.04
14 (Fig. 1b)	37/30 1.23 ± 0.03	31/23 1.35 ± 0.05	26/19 1.37 ± 0.06	9/9 1.00 (± 0.12)

ACKNOWLEDGMENTS

This work was partially supported by a grant from the Research and Publications Committee of the National University of Lesotho. RSS thanks the Council for the International Exchange of Scholars for a Fulbright Lectureship at the University of Lesotho during 1985–1986.

REFERENCES

Augustithis, S. S., 1982, Atlas of Sphaeroidal Textures and Structures and their Genetic Significance: Theophrastus Publications, Athens, Greece, p. 329.

Augustithis, S. S. and Ottemann, J., 1966, Diffusion rings and sphaeroidal weathering: Chem. Geol., v. 1, p. 201–209.

Augustithis, S. S.; Mposkos, E.; and Vgenopoulos, A., 1980, Diffusion rings (sphaeroids) in bauxite: Chem. Geol., v. 30, p. 351–362.

Burden, R. L.; Faires, J. D.; and Reynolds, A. C., 1981, Numerical Analysis: Prindle, Weber and Schmidt, Boston, Massachusetts, p. 180–257.

Carl, J. D. and Amstutz, G. C., 1958, Three-dimensional Liesegang rings by diffusion in a colloidal matrix, and their significance for the interpretation of geological phenomena: Bull. Geol. Soc. Amer., v. 69, p. 1467–1468.

Liesegang, R. E., 1913, Geologische Diffusionen: Dresden und Leipzig, Steinkopf, Germany, p. 180.

Matalon, R. and Packter, A., 1955, The Liesegang phenomenon I. Sol protection and diffusion: J. Colloid. Sci., v. 10, p. 46–62.

Packter, A., 1956a, The Liesegang phenomenon II. Addition of protecting agents: J. Colloid. Sci., v. 11, p. 96–106.

Packter, A., 1956b, The Liesegang phenomenon III. The structure of the gel medium: J. Colloid. Sci., v. 11, p. 150–157.

Singer, A. and Navrot, J., 1970, Diffusion rings in altered basalt: Chem. Geol., v. 6, p. 31–41.